Physica A 509 (2018) 620–634

Contents lists available at ScienceDirect

Physica A

journal homepage: www.elsevier.com/locate/physa

Degree distributions and motif profiles of limited penetrable horizontal visibility graphs

Minggang Wang [a,b,c], Hua Xu [b], Lixin Tian [a,*], H. Eugene Stanley [c]

[a] School of Mathematical Science, Nanjing Normal University, Nanjing 210042, Jiangsu, China
[b] Department of Mathematics, Nanjing Normal University Taizhou College, Taizhou 225300, Jiangsu, China
[c] Center for Polymer Studies and Department of Physics, Boston University, Boston, MA 02215, USA

HIGHLIGHTS

- We propose an intuitive method of reproducing the construction process of LPHVGs.
- We derive the degree distributions using iterative construction processes of LPHVGs.
- We introduce the sequential LPHVG motifs and present the exact motif profiles.
- We find the easy way to distinguish among different processes.

ARTICLE INFO

Article history:
Received 1 March 2018
Received in revised form 10 May 2018
Available online xxxx

Keywords:
Limited penetrable horizontal visibility graphs
Degree distribution
Motif profiles

ABSTRACT

The algorithm of limited penetrable horizontal visibility graphs (LPHVGs) including the limited penetrable horizontal visibility graph [LPHVG(ρ)], the directed limited penetrable horizontal visibility graph [DLPHVG(ρ)] and the image limited penetrable horizontal visibility graph [ILPHVG$_n$(ρ))] are used to map time series (or matrices) on graphs and are powerful tools for analyzing time series. We derive the degree distributions of LPHVGs using an iterative LPHVGs construction process. We propose a more intuitive method of reproducing the construction process of limited penetrable horizontal visibility graphs that is simple to calculate. We find that the results confirm the analytical results from previous methods. We then introduce the concept of sequential LPHVG(ρ) motifs and present a theoretical way of computing the exact motif profiles associated with unrelated random series. We perform several numerical simulations to further check the accuracy of our theoretical results. Finally we use the analytical results of LPHVG(ρ) motif profiles to distinguish among random, periodic, and chaotic signals and find that the frequency of the type-I motif captures sufficient information to easily distinguish among different processes.

1. Introduction

With the development of complex network theories [1–4], a new multidisciplinary methodology for characterizing nonlinear time series using complex network science has emerged and is now in are widely used [5–36]. Over the past decade several methodologies have been proposed for mapping a univariate and multivariate time series in a complex network using visibility graph algorithms [5–11], a recurrence network (RN) method [12–14], a stochastic processes method [15,16], a coarse geometry theory [17], a phase-space reconstruction method [18,19], and a phase-space coarse-graining method [20]. These methods have been widely used to solve problems in a variety of research fields [21–41].

* Corresponding author.
E-mail addresses: xuhua1590526@163.com (H. Xu), tianlx@ujs.edu.cn (L. Tian).

https://doi.org/10.1016/j.physa.2018.06.077
0378-4371/

Recently a limited penetrable visibility graph (LPVG) [42,43] and a multiscale limited penetrable horizontal visibility graph (MLPHVG) [44] were developed from the visibility graph (VG) and the horizontal visibility graph (HVG) to analyze nonlinear time series. The LPVG and LPHVG have been successfully used to analyze a variety of real signals across different fields, e.g., experimental flow signals [42] and electromechanical signals (EEG) [44–46]. Research has shown that the LPVG and LPHVG inherit the merits of the VG, but also successfully screen out noise, which makes them particularly useful when analyzing signals polluted by unavoidable noise [42–46].

A number of topological properties of the limited penetrable horizontal visibility graphs (LPHVGs) including the limited penetrable horizontal visibility graph [LPHVG(ρ)], the directed limited penetrable horizontal visibility graph [DLPHVG(ρ)] and the image limited penetrable horizontal visibility graph [ILPHVG$_n$(ρ))] mapped from time series of different complex systems have been studied numerically and analytically. The main contributions have come from Wang and his collaborators [47,48]. For example,Wang et al. [47] show that the random series maps on a LPHVG(ρ) with an exponential degree distribution $P(k) \sim exp[-\lambda(k-2\rho-2)]$, $\lambda = ln[(2\rho+3)/(2\rho+2)]$, $\rho = 0, 1, 2, \ldots,$ and $k = 2\rho+2, 2\rho+3, \ldots$, independent of the probability distribution from which the series was generated. They deduce the exact expressions of the mean degree and the clustering coefficient and demonstrate the long distance visibility property. Wang et al. [48] also extend LPHVG(ρ) and create a DLPHVG(ρ) and an ILPHVG$_n$(ρ)). They found that for the unrelated random series, the in- and out-degree distribution of its associated DLPHVG(ρ) follow the exponential degree distribution $P_{\text{in}}(k) = P_{\text{out}}(k) = \frac{1}{\rho+2}\left(\frac{\rho+1}{\rho+2}\right)^{k-(\rho+1)}$, $k \geq \rho+1$. The degree distribution $P(k)$ of the associated ILPHVG$_n$(ρ) converges to $\frac{1}{[n(\rho+1)+1]}\left[\frac{n(\rho+1)}{n(\rho+1)+1}\right]^{k-n(\rho+1)}$, $k \geq n(\rho+1)$.

We here propose an iterative approach to analytically deriving the degree distributions of LPHVG(ρ), DLPHVG(ρ) and ILPHVG$_n$(ρ). We derive the degree distributions of LPHVG(ρ), DLPHVG(ρ) and ILPHVG$_n$(ρ) mapped from random series that recover the results in Refs. [47] and [48]. We then introduce the sequential LPHVG motif concept and develop a theoretical way of exactly computing the motif profiles associated with unrelated random series. We perform several numerical simulations to further check the accuracy of our theoretical results. Finally we use the analytical results of LPHVG motif profiles to distinguish among random, periodic, and chaotic signals and find that the frequency of the type-I motif captures sufficient information to easily distinguish among different processes.

We organize the paper as follows. In Section 2 we describe LPHVG(ρ), DLPHVG(ρ) and ILPHVG$_n$(ρ). In Section 3 we derive the degree distributions using iterative construction processes LPHVG(ρ), DLPHVG(ρ) and ILPHVG$_n$(ρ). In Section 4 we introduce the concept of sequential LPHVG motifs, derive the motif profiles associated with unrelated random series, and present several numerical simulations to check their accuracy. In Section 5 we show a simple application of LPHVG motif profiles to distinguish among random, periodic and chaotic signals. In Section 6 we present our conclusions.

2. Construction of LPHVG(ρ), DLPHVG(ρ) and ILPHVG$_n$(ρ)

The limited penetrable horizontal visibility graph [LPHVG(ρ)] [47] is a geometrically simpler and analytically solvable version of VG [5], LPVG [42,43], and MLPHVG [44]. To define it we let $\{x_i\}_{i=1,2,\ldots,N}$ be a time series of N real numbers. We set the limited penetrable distance to ρ, and LPHVG(ρ) maps the time series on a graph with N nodes and an adjacency matrix $\mathbf{A}$. Nodes x_i and x_j are connected through an undirected edge ($A_{ij} = A_{ji} = 1$) if x_i and x_j have a limited penetrable horizontal visibility (see Fig. 1(a)), i.e., if $\rho \geq 0$ intermediate data x_q follows

$$x_q \geq inf\{x_i, x_j\}, \forall q \in (i, j), \aleph(q) \leq \rho, \tag{1}$$

where $\aleph(q)$ is the number of q. The graph spanned by this mapping is the limited penetrable horizontal visibility graph [LPHVG(ρ)]. When we set the limited penetrable distance ρ to 0, then LPHVG(0) degenerates into an HVG [6], i.e., LPHVG(0) = HVG. When $\rho \neq 0$ there are more connections between any two LPHVG(ρ) nodes than in HVG. Fig. 1(a) shows the new established connections (red lines) when we infer the LPHVG(1) using HVG.

The directed limited penetrable horizontal visibility graph [DLPHVG(ρ)] [48] can be defined by adding the directionality of LPHVG(ρ), where the degree $k(x_t)$ of the node x_t is split between an ingoing degree $k_{\text{in}}(x_t)$ and an outgoing degree $k_{\text{out}}(x_t)$ such that $k(x_t) = k_{\text{in}}(x_t) + k_{\text{out}}(x_t)$. We define the ingoing degree $k_{\text{in}}(x_t)$ to be the number of links of node x_t with past nodes associated with data in the series, i.e., nodes with $t' < t$. Conversely, we define the outgoing degree $k_{\text{out}}(x_t)$ to be the number of links with future nodes, i.e., nodes with $t'' > t$. Thus DLPHVG(ρ) maps the time series into a graph with N nodes and an adjacency matrix $\mathbf{A} = \mathbf{A}_{\text{in}} + \mathbf{A}_{\text{out}}$, where $\mathbf{A}_{\text{in}}$ is a lower triangular matrix and $\mathbf{A}_{\text{out}}$ is a upper triangular matrix. Nodes $x_{t'}$ and x_t, $t' < t$ (or x_t and $x_{t''}$, $t < t''$) are connected through a directed edge $x_{t'} \rightarrow x_t$, i.e., $A_{t't} = 1$ (or $x_t \rightarrow x_{t''}$, i.e., $A_{tt''} = 1$) if it satisfies Eq. (1). Fig. 1(b) shows a graphical representation of the definition. As in the degree distribution $P(k)$, we use the ingoing and outgoing degree distributions of a DLPHVG(ρ) to define the probability distributions of k_{out} and k_{in} on the graph, which are $P_{\text{out}}(k) \equiv P(k_{\text{out}} = k)$ and $P_{\text{in}}(k) \equiv P(k_{\text{in}} = k)$, respectively. We see the asymmetry of the resulting graph in a first approximation when we use the invariance of the outgoing (or ingoing) degree series under a time reversal.

The image limited penetrable horizontal visibility graph of order n [ILPHVG$_n$(ρ)] [48] is the extension of LPHVG(ρ). To define the image limited penetrable horizontal visibility graph of order n [ILPHVG$_n$(ρ)] we let $\mathbf{X}$ be a $N \times N$ matrix for an arbitrary entry (i, j) and partition the plane into n directions such that direction p is at an angle with the row axis of $2\pi(p-1)/n$, where $p = 1, 2, \ldots, n$. The image limited penetrable visibility graph of order n, ILPHVG$_n$(ρ), has N^2 nodes, each of which is labeled using a duple (i, j) associated with the entry indices x_{ij}, such that two nodes, x_{ij} and $x_{i'j'}$, are linked when

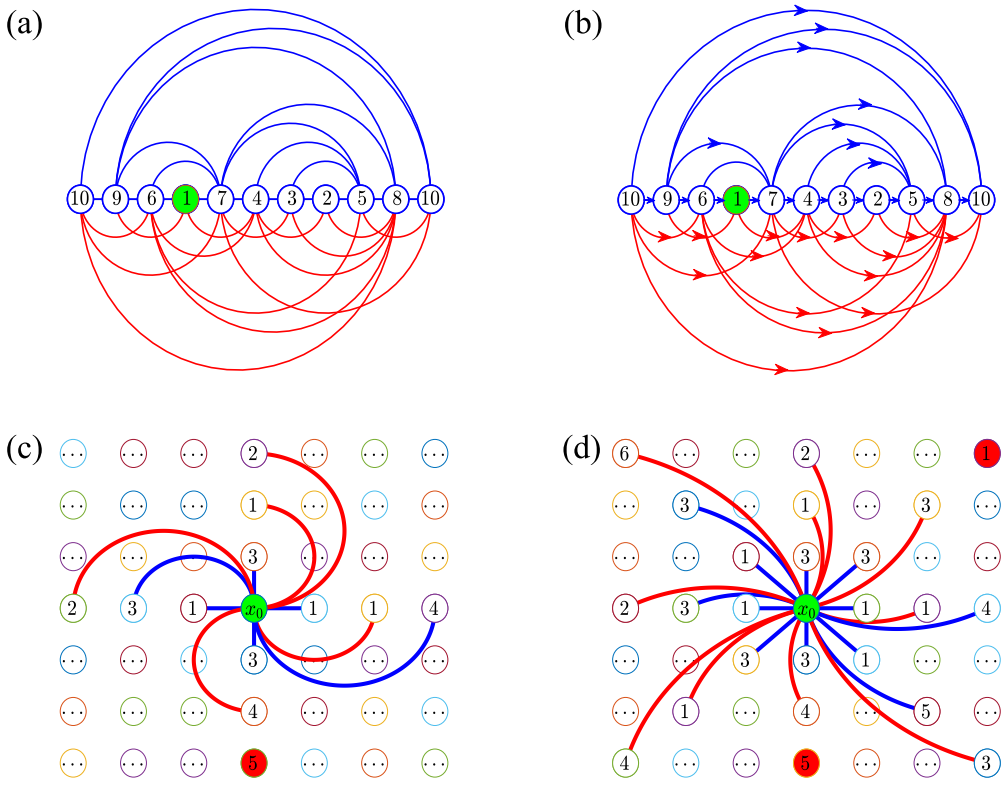

Fig. 1. Graphical illustration of LPHVGs (a) Example of a time series (11 data values) and its corresponding LPHVG(1), where every node corresponds to time series data in the same order. The horizontal penetrable visibility lines between data points define the links connecting nodes in the graph. (b) Graphical illustration of DLPHVG(1), where arrows, describing allowed directed penetrable visibility, link nodes. In this graph, each node has an ingoing degree k_{in}, which accounts for the number of links with past nodes, and an outgoing degree k_{out}, which in turn accounts for the number of links with future nodes. (c) we describe the connectivity pattern associated to this entry x_0 in the case of ILPHVG$_4$(1), which is evaluated along the vertical and horizontal directions. (d) we describe the connectivity pattern associated to this entry x_0 in the case of ILPHVG$_8$(1), which is evaluated both along the vertical and horizontal directions and along the diagonals directions. (For interpretation of the references to color in this figure legend, the reader is referred to the web version of this article.)

(i) $x_{i'j'}$ belongs to one of the n angular partition lines, and (ii) x_{ij} and $x_{i'j'}$ are linked in the LPHVG(ρ) defined over the ordered sequence that includes (i, j) and (i', j'). For example, in ILPHVG$_4$(1) the penetrable visibility between two points x_{ij} and $x_{i'j'}$ is

$$i = i', x_{iq} \geq inf\{x_{ij}, x_{i'j'}\}, \forall q \in (j, j'), \aleph(q) \leq \rho, \tag{2}$$

or

$$j = j', x_{qj} \geq inf\{x_{ij}, x_{i'j'}\}, \forall q \in (i, i'), \aleph(q) \leq \rho. \tag{3}$$

Fig. 1(c) shows a sample matrix in which x_0 is the central entry, which shows the ILPHVG$_4$(1) algorithm evaluated along the vertical and horizontal directions and the connectivity pattern associated to the entry x_0 of the ILPHVG$_4$(1) algorithm. Fig. 1(d) shows the ILPHVG$_8$(1) algorithm evaluated along the vertical, horizontal, and diagonal directions, and the connectivity pattern associated to the entry x_0 of the ILPHVG$_8$(1) algorithm.

3. Degree distributions associated to uncorrelated random time series

3.1. Degree distribution of LPHVG(ρ)

Wang et al. provided a detailed analysis and description about the degree distribution of the LPHVG(ρ) mapped from random time series [47]. Here we derive alternatively the theoretical function of degree distribution based on the master equation. Generating a time series of size N is equivalent to putting N numbers into N positions. In the first step, we randomly choose a position and put the largest number on it. In the second step, we choose a position from the rest $N - 1$ positions and put the second largest number on it. In step l, we randomly choose a position from the rest $N - l + 1$ positions and put the largest number l on it.

In general, we can construct an LPHVG(ρ) during the series generating process. For example, in step l, we have a series with a size of $l-1$ and we denote $L(k, l-1)$ the number of nodes with degree k in the corresponding LPHVG(ρ). When we put the last number into the series, the resulting LPHVG(ρ) will have l nodes. Because the last number is the smallest, only $2(\rho+1)$ new edges will be added to the LPHVG(ρ), as shown the green node in Fig. 1(a). (the case for $\rho = 1$) and these $2(\rho+1)$ new edges link to the $2(\rho+1)$ nodes adjacent to the node l. At the same time, the degree of each of the $2(\rho+1)$ nodes increase by 1. Since the new node is randomly placed, $l-1$ nodes have the same probability $2(\rho+1)/(l-1)$ of changing their degrees. Although node l can be placed at the first ρ or the last ρ of the $\rho-1$ nodes, when the number l is very large and $\rho \ll l$, i.e., $l \to \infty$, the probability of it happening is very small. We ignore the influence of these two extreme situations.

When a new node is added $2(\rho+1)$ the node degree increases by 1, from k to $k+1$, and the degrees of the remaining nodes are unchanged. The probability of a node degree change is $2(\rho+1)/(l-1)$ and the probability of degree not changing is $1-2(\rho+1)/(l-1)$. Hence the number of nodes with a degree k in the LPHVG(ρ) containing l nodes can be calculated

$$L(k, l) = [1 - \frac{2(\rho+1)}{l-1}]L(k, l-1) + \frac{2(\rho+1)}{l-1}L(k-1, l-1) + \delta_{k2(\rho+1)}. \tag{4}$$

where

$$\delta_{k2(\rho+1)} = \begin{cases} 1, k = 2\rho+2, \\ 0, otherwise, \end{cases}$$

because the degree of each new node is $k = 2(\rho+1)$. We define the probability of nodes with degree k in the LPHVG(ρ) containing l nodes

$$P(k, l) = L(k, l)/l. \tag{5}$$

Hence, Eq. (4) can be rewritten

$$P(k, l) \approx \left(1 - \frac{3+2\rho}{l}\right) P(k, l-1) + \frac{2(\rho+1)}{l}P(k-1, l-1), \tag{6}$$

in which $\delta_{k2(\rho+1)}/l = 0$ for large l. When $l \to \infty$, we have

$$\begin{cases} P(k-1, l) = P(k-1, l-1) = P(k-1), \\ P(k, l) = P(k, l-1) = P(k). \end{cases} \tag{7}$$

Combining Eqs. (6) and (7), we obtain

$$P(k) = \frac{2\rho+2}{2\rho+3}P(k-1). \tag{8}$$

By applying $\sum_{k=2(\rho+1)}^{\infty} P(k) = 1$, we obtain the solution of Eq. (8)

$$P(k) = \frac{(2\rho+3)^{2\rho+1}}{(2\rho+2)^{2\rho+2}} \left(\frac{2\rho+2}{2\rho+3}\right)^k \tag{9}$$

This result is consistent with the analytical expression in Refs. [47,48].

3.2. Degree distributions of DLPHVG(ρ)

The degree distribution of a DLPHVG(ρ) can also be derived by using a construction process for the DLPHVG(ρ) that is iterative. As when deriving LPHVG(ρ), we construct a directed LPHVG(ρ) from a time series with $l-1$ numbers in step l. We define $L_D(k, l-1)$ to be the number of nodes with an in- or out-degree k. Fig. 1(b) shows that when we add the largest number l into the DLPHVG(ρ), $2(\rho+1)$ new edges are generated (green) – $\rho+1$ out-edges and $\rho+1$ in-edges – and they link to the $2(\rho+1)$ nodes adjacent to node l. The out-degree of the left node and the in-degree of the right node increase by 1. Because the new node is placed randomly, with a probability $(\rho+1)/(l-1)$ one end point of a node in-degree or out-degree increases by 1. With a probability of $1-(\rho+1)/(l-1)$ the other node degrees remain the same. Thus the number of nodes with degree k in the new DLPHVG(ρ) containing l nodes is

$$L_D(k, l) = \left(1 - \frac{\rho+1}{l-1}\right) L_D(k, l-1) + \frac{\rho+1}{l-1}L_D(k-1, l-1) + \delta_{k(\rho+1)}. \tag{10}$$

where

$$\delta_{k(\rho+1)} = \begin{cases} 1, k = \rho+1, \\ 0, otherwise, \end{cases}$$

because the degree of each new node is $k = \rho + 1$. When $k = \rho + 1$,then $\delta_{k(\rho+1)} = 1$. When $k \neq \rho + 1$, then $\delta_{k(\rho+1)} = 0$. We define $P_D(k) = L_D(k, l)/l$ the probability of nodes with the in-degree or out-degree k in the DLPHVG(ρ) containing l nodes. Thus Eq. (10) can be rewritten

$$P_D(k, l) = \left(1 - \frac{\rho + 2}{l}\right) P_D(k, l - 1) + \frac{\rho + 1}{l} P_D(k - 1, l - 1). \tag{11}$$

When $l \to \infty$, we have

$$\begin{cases} P_D(k - 1, l) = P_D(k - 1, l - 1) = P_D(k - 1), \\ P_D(k, l) = P_D(k, l - 1) = P_D(k). \end{cases} \tag{12}$$

Combining Eqs. (11) and (12), we obtain

$$P_D(k) = \frac{\rho + 1}{\rho + 2} P_D(k - 1). \tag{13}$$

By applying $\sum_{k=\rho+1}^{\infty} P_D(k) = 1$, we obtain the solution to Eq. (13)

$$P(k) = \frac{(\rho + 2)^{\rho}}{(\rho + 1)^{\rho+1}} \left(\frac{\rho + 1}{\rho + 2}\right)^{k}. \tag{14}$$

This result is consistent with the analytical expression in Ref. [48].

3.3. Degree distributions of ILPHVG$_n$(ρ)

To derive the general results of a ILPHVG$_n$(ρ) using iterative construction process, we first examine the two special cases $n = 4$ and $n = 8$.

When $n = 4$, as in the derivation process of LPHVG(ρ) we construct the ILPHVG$_n$(ρ) from a matrix with $l^2 - 1$ numbers in step l^2. We define $L_l(k, l^2 - 1)$ the number of nodes with degree k. When we add largest number l^2 into the ILPHVG$_4$(ρ), only $4(\rho + 1)$ new edges are generated shown as the green node in Fig. 2(a) ($\rho = 0$), Fig. 2(b) ($\rho = 1$), Fig. 2(c) ($\rho = 2$) and the $4(\rho + 1)$ new edges link to the $4(\rho + 1)$ nodes adjacent to node l^2. The degree of each $4(\rho + 1)$ node increases by 1. Because the new node is placed randomly, $l^2 - 1$ nodes have the same probability $4(\rho + 1)/(l^2 - 1)$ of changing their degrees. With a probability $1 - 4(\rho + 1)/(l^2 - 1)$ the other node degrees remain the same. So the number of nodes with degree k in the new ILPHVG$_4$(ρ) containing l^2 nodes is

$$L_{l4}(k, l^2) = \left[1 - \frac{4(\rho + 1)}{l^2 - 1}\right] L_{l4}(k, l^2 - 1) + \frac{4(\rho + 1)}{l^2 - 1} L_{l4}(k - 1, l^2 - 1) + \delta_{k4(\rho+1)}. \tag{15}$$

where

$$\delta_{k4(\rho+1)} = \begin{cases} 1, k = 4\rho + 4, \\ 0, otherwise, \end{cases}$$

because the degree of each new node is $k = 4(\rho + 1)$. The probability that nodes with degree k in the ILHVG$_4$(ρ) containing l^2 nodes is calculated

$$P_{l4}(k, l^2) = L_{l4}(k, l^2)/l^2. \tag{16}$$

Thus we rewrite Eq. (15) to be

$$P_{l4}(k, l^2) \approx \left(1 - \frac{4\rho + 5}{l^2}\right) P_{l4}(k, l^2 - 1) + \frac{4(\rho + 1)}{l^2} P_{l4}(k - 1, l^2 - 1), \tag{17}$$

in which $\delta_{k2(\rho+1)}/l^2 = 0$ for large l^2. When $l^2 \to \infty$, we have

$$\begin{cases} P_{l4}(k - 1, l^2) = P_{l4}(k - 1, l^2 - 1) = P_{l4}(k - 1), \\ P_{l4}(k, l^2) = P_{l4}(k, l^2 - 1) = P_{l4}(k). \end{cases} \tag{18}$$

Combining Eqs. (17) and (18) we obtain

$$P_{l4}(k) = \frac{4\rho + 4}{4\rho + 5} P_{l4}(k - 1). \tag{19}$$

By applying $\sum_{k=4(\rho+1)}^{\infty} P_{l4}(k) = 1$ we obtain the solution to Eq. (19)

$$P_{l4}(k) = \frac{(4\rho + 5)^{4\rho+3}}{(4\rho + 4)^{4\rho+4}} \left(\frac{4\rho + 4}{4\rho + 5}\right)^{k}. \tag{20}$$

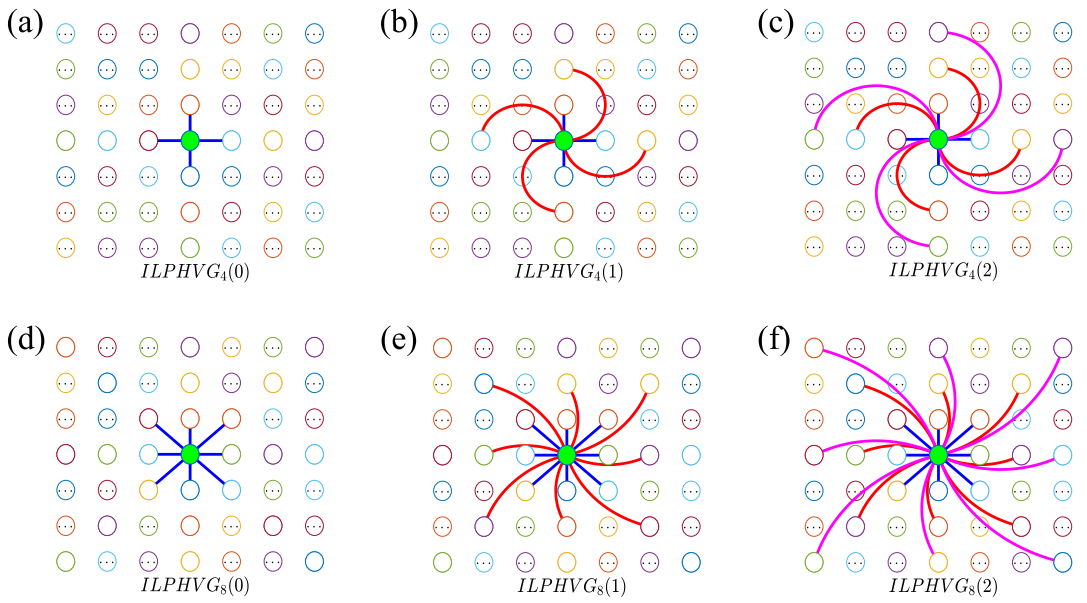

Fig. 2. Graphical illustration of the new edges generated of ILPHVG$_4(\rho)$ and ILPHVG$_8(\rho)$ with $\rho = 0, 1, 2$ when we add the l^2-th largest number (the green node) into ILPHVG$_4(\rho)$ and ILPHVG$_8(\rho)$. (For interpretation of the references to color in this figure legend, the reader is referred to the web version of this article.)

Similarly, when $n = 8$ we add the largest number l^2 into the ILPHVG$_8(\rho)$, and $8(\rho + 1)$ new edges are generated, i.e., the green node in Fig. 2(d) ($\rho = 0$), Fig. 2(e) ($\rho = 1$), and Fig. 2(f) ($\rho = 2$) and $8(\rho+1)$ new edges link to $8(\rho+1)$ nodes adjacent to node l^2. We then change Eq. (15) to

$$L_{I8}(k, l^2) = \left[1 - \frac{8(\rho+1)}{l^2-1}\right] L_{I8}(k, l^2-1) + \frac{8(\rho+1)}{l^2-1} L_{I8}(k-1, l^2-1) + \delta_{k8(\rho+1)}. \tag{21}$$

Thus

$$P_{I8}(k, l^2) \approx \left(1 - \frac{8\rho+9}{l^2}\right) P_{I8}(k, l^2-1) + \frac{8(\rho+1)}{l^2} P_{I8}(k-1, l^2-1), \tag{22}$$

When $l^2 \to \infty$, we have

$$P_{I8}(k) = \frac{8\rho+8}{8\rho+9} P_{I8}(k-1). \tag{23}$$

By applying $\sum_{k=8(\rho+1)}^{\infty} P_{I8}(k) = 1$ we obtain the solution to Eq. (23)

$$P_{I8}(k) = \frac{(8\rho+9)^{8\rho+7}}{(8\rho+8)^{8\rho+8}} \left(\frac{8\rho+8}{8\rho+9}\right)^k. \tag{24}$$

From Eq. (20) and (24), we deduce a generic n that yields

$$P_{In}(k) = \frac{[n(\rho+1)+1]^{n(\rho+1)-1}}{[n(\rho+1)]^{n(\rho+1)}} \left[\frac{n(\rho+1)}{n(\rho+1)+1}\right]^k. \tag{25}$$

This result is also consistent with the analytical expression in Ref. [48].

On the above work, we propose a method of deriving the degree distributions of the limited penetrable horizontal visibility graphs, including LPHVG(ρ), DLPHVG(ρ) and ILPHVG$_n(\rho)$ using an iterative construction process for all three. In contrast with previous methods [45,46], this method reproduces the construction process of the limited penetrable horizontal visibility graphs, and it is more intuitive and the calculation process simpler.

4. Sequential motif profile of limited penetrable horizontal visibility graphs

Iacovacci and his collaborators [9,10] recently introduced the concept of sequential VG and HVG motifs and proposed a theory of exactly computing $\mathbf{Z}^4$ in VG and HVG. They demonstrated that using the 4-motif statistics allows us to discriminate between different types of dynamical and stochastic processes. We extend their results [9,10] and introduce sequential

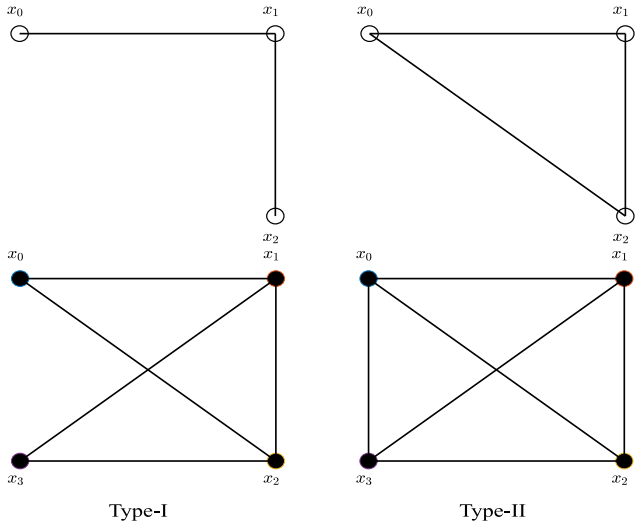

Fig. 3. All $(\rho + 3)$-node motifs of LPHVG(ρ) with$\rho = 0$ (the upper) and $\rho = 1$ (the bottom).

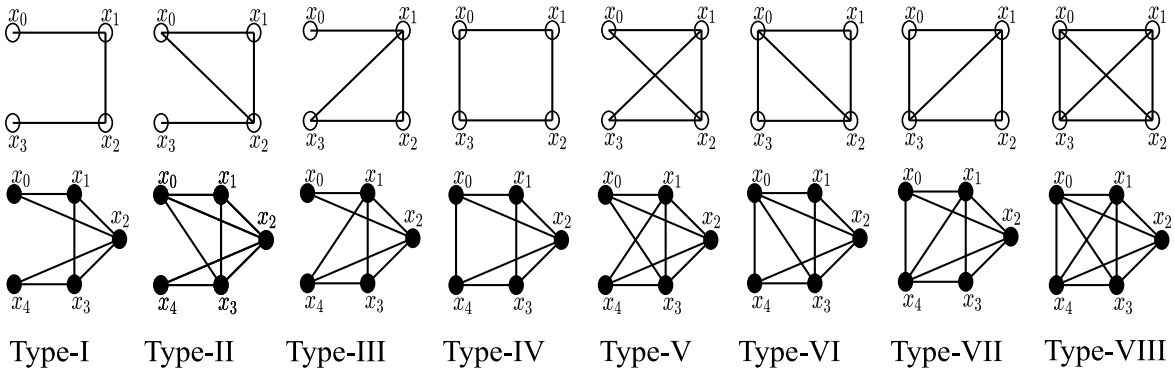

Fig. 4. All $(\rho + 4)$-node motifs of LPHVG(ρ)with$\rho = 0$ (the upper) and $\rho = 1$ (the bottom). Note that when $\rho = 0$, the type-V and type-VIII motifs are actually not admissible under the HVG algorithm.

$(\rho + n)$-node motifs for LPHVG(ρ). We examine a LPHVG(ρ) of N nodes associated with a time series of N data and label the nodes according to the natural ordering induced by the time direction. We set $(\rho + n) < N$ and consider sequentially all the subgraphs formed by the sequence of nodes $\{\tau, \tau + 1, \ldots, \tau + \rho + n - 1\}$ (where τ is an integer that takes values in [1,N-ρ-n+1]), and the edges from the LPHVG(ρ) connect the nodes. We define them to be the sequential $(\rho + n)$-node motifs of the LPHVG(ρ). Figs. 3 and 4 show all the $(\rho + 3)$-node and $(\rho + 4)$-node motifs of LPHVG(ρ) with $\rho = 0,1$. Note that the $(\rho + 3)$-node motifs include the Type-I and Type-II motifs, and that $(\rho + 4)$-node motifs include the Type-I, Type-II, Type-III, Type-IV, Type-V, Type-VI, Type-VII and Type-VIII motifs. Note that for $(\rho + 4)$-node motifs, when $\rho = 0$ the Type-V and Type-VIII motifs are not admissible under the HVG algorithm, i.e., there are only six admissible 4-node motifs of HVG [9], but when $\rho > 0$, the Type-V and Type-VIII motifs are both admissible.

As in Refs. [9] and [10], we compare the LPHVG(ρ)s associated with different time series and dynamics by comparing the relative occurrence of each motif inside a LPHVG(ρ). To do so we add to LPHVG(ρ) a significance profile [named LPHVG(ρ) motif profile $\mathbf{Z}^{\rho+n}$]. Let p be the total number of admissible LPHVG(ρ) motifs with $\rho + n$ nodes. We assign to each p motif a label from 1 to p (see Figs. 3 and 4), and define the LPHVG(ρ) motif profile $\mathbf{Z}^{\rho+n}$ of a time series of size N to be the vector function

$$\mathbf{Z}^{\rho+n} : (\rho + n) \in \mathbb{N} \rightarrow [P_1^{\rho+n}, \ldots, P_p^{\rho+n}], \tag{26}$$

whose output is a vector of p components, where component i, $P_i^{\rho+n}$, is the relative frequency of the type-i motif. We next compute the frequency of each LPHVG(ρ) motif. We examine a generic dynamical process $\mathcal{H} : \mathbb{R} \rightarrow \mathbb{R}$ with a smooth invariant measure $f(x), x \in [a, b]$ that fulfills the Markov property $f(x_\tau|x_{\tau-1}, x_{\tau-2}, \ldots) = f(x_\tau|x_{\tau-1})$, where $f(x_\tau|x_{\tau-1})$ is the transition probability distribution [9,10]. Each LPHVG(ρ) motif has a probability of appearance as a subgraph that is determined by measuring the set of ordering inequalities that occur in the time series. For example, the LPHVG(ρ) motif

profile $\mathbf{Z}^{\rho+3} = [P_I^{\rho+3}, P_{II}^{\rho+3}]$ is

$$P_i^{\rho+3} = \int\int \dots \int f(x_\tau) f(x_{\tau+1}|x_\tau) \dots f(x_{\tau+\rho+2}|x_{\tau+\rho+1}) dx_{\tau+\rho+2} \dots dx_{\tau+1} dx_\tau . \tag{27}$$

Using Eq. (27) to examine the independent and identically distributed (*i.i.d.*) random time series, for the $(\rho+3)-$ node motif, we obtain the following:

Theorem 1. *Consider a bi-infinite series of i.i.d. random variable extracted from a continuous distribution $f(x)$ with support (a, b), where $a, b \in \mathbb{R}$. Then the probability of finding the $(\rho+3)-$ node motif of LPHVG(ρ) converges to $\left[\frac{2}{\rho+3}, \frac{\rho+1}{\rho+3}\right]$, i.e.,*

$$\lim_{N\to\infty} \mathbf{Z}^{\rho+3} = \left[\frac{2}{\rho+3}, \frac{\rho+1}{\rho+3}\right].$$

Proof. Ref. [9] provides a constructive proof of the special case ($\rho = 0$) of this theorem. We here derive the general case. Fig. 3 shows both undirected motifs of $(\rho+3)$-nodes with $\rho = 0,1$. Note that there are only two types of motifs for $(\rho+3)$-nodes only have two types. We here first calculate the probability of Type-II ($P_{II}^{\rho+3}$).

We first consider $\rho = 1$. Here the motif of Type-II can be characterized using a hierarchy of inequalities in the associated time series and the union sets of the three exclusive inequality sets

$$S_{II}^{1+3} = \{\forall x_0, x_1 < x_0, x_2 < x_1, x_3 > x_2\} \cup \{\forall x_0, x_1 < x_0, x_2 > x_1, x_3 > x_1\} \cup \{\forall x_0, x_1 > x_0, x_2 < x_0, x_3 > x_2\}. \tag{28}$$

We define the cumulative probability distribution function $F(x)$ of any probability density $f(x)$ to be

$$F(x) = \int_a^x f(t)dt, F(a) = 0, F(b) = 1. \tag{29}$$

Using Eqs. (27) and (29), the probability of Eq. (28) is

$$\begin{aligned} P_{II}^{1+3} = &\int_a^b f(x_0)dx_0 \int_a^{x_0} f(x_1)dx_1 \int_a^{x_1} f(x_2)dx_2 \int_{x_2}^b f(x_3)dx_3 + \int_a^b f(x_0)dx_0 \int_a^{x_0} f(x_1)dx_1 \int_{x_1}^b f(x_2)dx_2 \int_{x_1}^b f(x_3)dx_3 \\ &+ \int_a^b f(x_0)dx_0 \int_{x_0}^b f(x_1)dx_1 \int_a^{x_0} f(x_2)dx_2 \int_{x_2}^b f(x_3)dx_3 = \frac{1}{2}. \end{aligned} \tag{30}$$

When $\rho = 2$, we characterize the motif of Type-II using the union sets of the seven exclusive inequality sets

$$\begin{aligned} S_{II}^{2+3} = &\{\forall x_0, x_1 < x_0, x_2 < x_1, x_3 < x_2, x_4 > x_3\} \cup \{\forall x_0, x_1 < x_0, x_2 < x_1, x_3 > x_2, x_4 > x_2\} \\ &\cup \{\forall x_0, x_1 < x_0, x_2 > x_1, x_3 > x_1, x_4 > x_1\} \cup \{\forall x_0, x_1 < x_0, x_2 > x_1, x_3 < x_1, x_4 > x_3\} \\ &\cup \{\forall x_0, x_1 > x_0, x_2 > x_0, x_3 < x_0, x_4 > x_3\} \cup \{\forall x_0, x_1 > x_0, x_2 < x_0, x_3 < x_2, x_4 > x_3\} \\ &\cup \{\forall x_0, x_1 > x_0, x_2 < x_0, x_3 > x_2, x_4 > x_2\}. \end{aligned} \tag{31}$$

The probability of this event occurring is

$$\begin{aligned} P_{II}^{2+3} = &\int_a^b f(x_0)dx_0 \int_a^{x_0} f(x_1)dx_1 \int_a^{x_1} f(x_2)dx_2 \int_a^{x_2} f(x_3)dx_3 \int_{x_3}^b f(x_4)dx_4 + \int_a^b f(x_0)dx_0 \int_a^{x_0} f(x_1)dx_1 \\ &\times \int_a^{x_1} f(x_2)dx_2 \int_{x_2}^b f(x_3)dx_3 \int_{x_2}^b f(x_4)dx_4 + \int_a^b f(x_0)dx_0 \int_a^{x_0} f(x_1)dx_1 \int_{x_1}^b f(x_2)dx_2 \int_{x_1}^b f(x_3)dx_3 \int_{x_1}^b f(x_4)dx_4 \\ &+ \int_a^b f(x_0)dx_0 \int_a^{x_0} f(x_1)dx_1 \int_{x_1}^b f(x_2)dx_2 \int_a^{x_1} f(x_3)dx_3 \int_{x_3}^b f(x_4)dx_4 + \int_a^b f(x_0)dx_0 \int_{x_0}^b f(x_1)dx_1 \int_{x_0}^b f(x_2)dx_2 \\ &\times \int_a^{x_0} f(x_3)dx_3 \int_{x_3}^b f(x_4)dx_4 + \int_a^b f(x_0)dx_0 \int_{x_0}^b f(x_1)dx_1 \int_a^{x_0} f(x_2)dx_2 \int_a^{x_2} f(x_3)dx_3 \int_{x_3}^b f(x_4)dx_4 \\ &+ \int_a^b f(x_0)dx_0 \int_{x_0}^b f(x_1)dx_1 \int_a^{x_0} f(x_2)dx_2 \int_{x_2}^b f(x_3)dx_3 \int_{x_2}^b f(x_4)dx_4 = \frac{3}{5}. \end{aligned} \tag{32}$$

In the same way we characterize the motif of Type-II using the union sets of the $\sum_{i=0}^{\rho} 2^i$ exclusive inequality sets

$$\begin{aligned}
S_{II}^{\rho+3} &= \{\forall x_0, x_1 < x_0, x_2 < x_1, x_3 < x_2, \ldots, x_{\rho-1} < x_{\rho-2}, x_\rho < x_{\rho-1}, x_{\rho+1} < x_\rho, x_{\rho+2} > x_{\rho+1}\} \\
&\cup \{\forall x_0, x_1 < x_0, x_2 < x_1, x_3 < x_2, \ldots, x_{\rho-1} < x_{\rho-2}, x_\rho < x_{\rho-1}, x_{\rho+1} > x_\rho, x_{\rho+2} > x_\rho\} \\
&\cup \{\forall x_0, x_1 < x_0, x_2 < x_1, x_3 < x_2, \ldots, x_{\rho-1} < x_{\rho-2}, x_\rho > x_{\rho-1}, x_{\rho+1} > x_{\rho-1}, x_{\rho+2} > x_{\rho-1}\} \\
&\cup \{\forall x_0, x_1 < x_0, x_2 < x_1, x_3 < x_2, \ldots, x_{\rho-1} < x_{\rho-2}, x_\rho > x_{\rho-1}, x_{\rho+1} < x_{\rho-1}, x_{\rho+2} > x_{\rho+1}\} \\
&\cup \cdots \cup \{\forall x_0, x_1 < x_0, x_2 > x_1, x_3 > x_1, \ldots, x_{\rho-1} > x_1, x_\rho > x_1, x_{\rho+1} > x_1, x_{\rho+2} > x_1\} \\
&\cup \cdots \cup \{\forall x_0, x_1 < x_0, x_2 > x_1, x_3 < x_1, \ldots, x_{\rho+1} > x_\rho, x_{\rho+2} > x_\rho\} \\
&\cup \{\forall x_0, x_1 > x_0, x_2 > x_0, x_3 > x_0, \ldots, x_\rho > x_0, x_{\rho+1} < x_\rho, x_{\rho+2} > x_{\rho+1}\} \\
&\cup \{\forall x_0, x_1 > x_0, x_2 > x_0, x_3 > x_0, \ldots, x_\rho < x_0, x_{\rho+1} < x_\rho, x_{\rho+2} > x_{\rho+1}\} \\
&\cup \{\forall x_0, x_1 > x_0, x_2 > x_0, x_3 > x_0, \ldots, x_\rho < x_0, x_{\rho+1} > x_\rho, x_{\rho+2} > x_\rho\} \\
&\cup \cdots \cup \{\forall x_0, x_1 > x_0, x_2 < x_0, x_3 > x_2, \ldots, x_\rho > x_2, x_{\rho+1} > x_2, x_{\rho+2} > x_2\}.
\end{aligned} \tag{33}$$

The probability of this event occurring is

$$\begin{aligned}
P_\rho(II)^{\rho+3} &= \int_a^b f(x_0)dx_0 \int_a^{x_0} f(x_1)dx_1 \int_a^{x_1} f(x_2)dx_2 \int_a^{x_2} f(x_3)dx_3 \ldots \int_a^{x_{\rho-1}} f(x_\rho)dx_\rho \\
&\times \int_a^{x_\rho} f(x_{\rho+1})dx_{\rho+1} \int_{x_{\rho+1}}^b f(x_{\rho+2})dx_{\rho+2} \\
&+ \int_a^b f(x_0)dx_0 \int_a^{x_0} f(x_1)dx_1 \int_a^{x_1} f(x_2)dx_2 \int_a^{x_2} f(x_3)dx_3 \ldots \int_a^{x_{\rho-1}} f(x_\rho)dx_\rho \int_{x_\rho}^b f(x_{\rho+1})dx_{\rho+1} \int_{x_\rho}^b f(x_{\rho+2})dx_{\rho+2} \\
&+ \int_a^b f(x_0)dx_0 \int_a^{x_0} f(x_1)dx_1 \int_a^{x_1} f(x_2)dx_2 \int_a^{x_2} f(x_3)dx_3 \ldots \int_{x_{\rho-1}}^b f(x_\rho)dx_\rho \int_{x_{\rho-1}}^b f(x_{\rho+1})dx_{\rho+1} \int_{x_{\rho-1}}^b f(x_{\rho+2})dx_{\rho+2} \\
&+ \int_a^b f(x_0)dx_0 \int_a^{x_0} f(x_1)dx_1 \int_a^{x_1} f(x_2)dx_2 \int_a^{x_2} f(x_3)dx_3 \ldots \int_{x_{\rho-1}}^b f(x_\rho)dx_\rho \int_a^{x_{\rho-1}} f(x_{\rho+1})dx_{\rho+1} \int_{x_{\rho+1}}^b f(x_{\rho+2})dx_{\rho+2} \\
&+ \cdots + \int_a^b f(x_0)dx_0 \int_a^{x_0} f(x_1)dx_1 \int_{x_1}^b f(x_2)dx_2 \int_{x_1}^b f(x_3)dx_3 \ldots \int_{x_1}^b f(x_\rho)dx_\rho \int_{x_1}^b f(x_{\rho+1})dx_{\rho+1} \int_{x_1}^b f(x_{\rho+2})dx_{\rho+2} \\
&+ \cdots + \int_a^b f(x_0)dx_0 \int_a^{x_0} f(x_1)dx_1 \int_{x_1}^b f(x_2)dx_2 \int_a^{x_1} f(x_3)dx_3 \ldots \int_{x_\rho}^b f(x_{\rho+1})dx_{\rho+1} \int_{x_\rho}^b f(x_{\rho+2})dx_{\rho+2} \\
&+ \int_a^b f(x_0)dx_0 \int_a^{x_0} f(x_1)dx_1 \int_{x_0}^b f(x_2)dx_2 \int_{x_0}^b f(x_3)dx_3 \ldots \int_{x_0}^b f(x_\rho)dx_\rho \int_a^{x_\rho} f(x_{\rho+1})dx_{\rho+1} \int_{x_{\rho+1}}^b f(x_{\rho+2})dx_{\rho+2} \\
&+ \int_a^b f(x_0)dx_0 \int_a^{x_0} f(x_1)dx_1 \int_{x_0}^b f(x_2)dx_2 \int_{x_0}^b f(x_3)dx_3 \ldots \int_a^{x_0} f(x_\rho)dx_\rho \int_a^{x_\rho} f(x_{\rho+1})dx_{\rho+1} \int_{x_{\rho+1}}^b f(x_{\rho+2})dx_{\rho+2} \\
&+ \int_a^b f(x_0)dx_0 \int_a^{x_0} f(x_1)dx_1 \int_{x_0}^b f(x_2)dx_2 \int_{x_0}^b f(x_3)dx_3 \ldots \int_a^{x_0} f(x_\rho)dx_\rho \int_{x_\rho}^b f(x_{\rho+1})dx_{\rho+1} \int_{x_\rho}^b f(x_{\rho+2})dx_{\rho+2} \\
&+ \cdots + \int_a^b f(x_0)dx_0 \int_a^{x_0} f(x_1)dx_1 \int_a^{x_0} f(x_2)dx_2 \int_{x_2}^b f(x_3)dx_3 \ldots \int_{x_2}^b f(x_\rho)dx_\rho \\
&\times \int_{x_2}^b f(x_{\rho+1})dx_{\rho+1} \int_{x_2}^b f(x_{\rho+2})dx_{\rho+2} = \frac{\rho+1}{\rho+2}.
\end{aligned} \tag{34}$$

Thus, $P_I^{\rho+3} = 1 - P_{II}^{\rho+3} = 1 - \frac{\rho+1}{\rho+2} = \frac{2}{\rho+3}$, that is,

$$\lim_{N\to\infty} \mathbf{Z}^{\rho+3} = \left[\frac{2}{\rho+3}, \frac{\rho+1}{\rho+3}\right]. \tag{35}$$

Note that when $\rho \to \infty$, $P_{II}^{\rho+3} \to 1$, i.e., $\mathbf{Z}^{\rho+3} \to [0, 1]$.

Note that $\mathbf{Z}^3$ does not capture enough structure for distinguishing the chaotic logistic map and *i.i.d.* series [9]. We here test whether $\mathbf{Z}^{\rho+3}$, $\rho \geq 1$ can capture enough structure for distinguishing both processes. We calculate $\mathbf{Z}^{1+3}$ for the chaotic logistic map

$$\hbar(x) = 4x(1-x), x \in [0, 1], f(x) = \frac{1}{\pi\sqrt{x(1-x)}}.$$

In this case,

$$\begin{aligned} P_{II}^{1+3} &= \int_0^1 f(x_0)dx_0 \int_0^{x_0} \delta(x_1 - \hbar(x_0))dx_1 \int_0^{x_1} \delta(x_2 - \hbar^2(x_0))dx_2 \int_{x_2}^1 \delta(x_3 - \hbar^3(x_0))dx_3 \\ &+ \int_0^1 f(x_0)dx_0 \int_0^{x_0} \delta(x_1 - \hbar(x_0))dx_1 \int_{x_1}^1 \delta(x_2 - \hbar^2(x_0))dx_2 \int_{x_1}^1 \delta(x_3 - \hbar^3(x_0))dx_3 \\ &+ \int_0^1 f(x_0)dx_0 \int_{x_0}^b \delta(x_1 - \hbar(x_0))dx_1 \int_0^{x_0} \delta(x_2 - \hbar^2(x_0))dx_2 \int_{x_2}^1 \delta(x_3 - \hbar^3(x_0))dx_3 \\ &= P_1 + P_2 + P_3, \end{aligned} \tag{36}$$

where

$$\int_0^1 \delta(x - y)dx = \begin{cases} 1, y \in [0, 1], \\ 0, otherwise. \end{cases} \tag{37}$$

Since the Dirac-delta integrals only have the effects of shrinking the range of integration of x_0, thus for P_1, the integral in x_1 requires (see Fig. 5(a))

$$[\hbar(x_0) < x_0] \cap [0, 1] \Rightarrow x_0 \in [3/4, 1], \tag{38}$$

the integral in x_2 requires

$$[\hbar^2(x_0) < \hbar(x_0)] \cap [3/4, 1] \Rightarrow x_0 \in [1/4, 3/4] \cap [3/4, 1] = \emptyset, \tag{39}$$

the integral in x_3 requires

$$[\hbar^3(x_0) > \hbar^2(x_0)] \cap \emptyset \Rightarrow x_0 = \emptyset. \tag{40}$$

thus, $P_1 = 0$.

For P_2, the integral in x_1 requires

$$[\hbar(x_0) < x_0] \cap [0, 1] \Rightarrow x_0 \in [3/4, 1], \tag{41}$$

the integral in x_2 requires

$$[\hbar^2(x_0) > \hbar(x_0)] \cap [3/4, 1] \Rightarrow x_0 \in ([0, 1/4] \cup [3/4, 1]) \cap [3/4, 1] \Rightarrow x_0 \in [3/4, 1], \tag{42}$$

the integral in x_3 requires

$$\begin{aligned} &[\hbar^3(x_0) > \hbar(x_0)] \cap [3/4, 1] \\ &\Rightarrow x_0 \in ([0, (3 - \sqrt{5})/8] \cup [1/4, (3 + \sqrt{5})/8] \cup [(5 - \sqrt{5})/8, 3/4] \cup [(5 + \sqrt{5})/8, 1]) \cap [3/4, 1] \\ &\Rightarrow x_0 \in [(5 + \sqrt{5})/8, 1], \end{aligned} \tag{43}$$

thus, $P_2 = \int_{(5+\sqrt{5})/8}^1 f(x_0)dx_0 = 1/5$.

For P_3, the integral in x_1 requires

$$[\hbar(x_0) > x_0] \cap [0, 1] \Rightarrow x_0 \in [0, 3/4], \tag{44}$$

the integral in x_2 requires

$$\begin{aligned} &[\hbar(x_0) < x_0] \cap [0, 3/4] \\ &\Rightarrow x_0 \in ([(5 - \sqrt{5})/8, 3/4] \cup [(5 + \sqrt{5})/8, 1]) \cap [0, 3/4] \Rightarrow x_0 \in [(5 - \sqrt{5})/8, 3/4], \end{aligned} \tag{45}$$

the integral in x_3 requires

$$\begin{aligned} &[\hbar^3(x_0) > \hbar^2(x_0)] \cap [(5 - \sqrt{5})/8, 3/4] \\ &\Rightarrow x_0 \in ([0, (2 - \sqrt{3})/4] \cup [1/4, 3/4] \cup [(2 + \sqrt{3})/4, 1]) \cap [(5 - \sqrt{5})/8, 3/4] \\ &\Rightarrow x_0 \in [(5 - \sqrt{5})/8, 3/4], \end{aligned} \tag{46}$$

thus, $P_3 = \int_{(5-\sqrt{5})/8}^{3/4} f(x_0)dx_0 = 4/15$. Therefore, $P_{II}^{1+3} = P_1 + P_2 + P_3 = \frac{14}{30}$, which is indeed quite different from the result for *i.i.d.* (Eq. (30)). This result demonstrates $\mathbf{Z}^{1+3}$ can capture enough structure for distinguishing the logistic map and *i.i.d.* series. In fact, for chaotic logistic map we can also obtain

$$\lim_{N\to\infty} \mathbf{Z}^{\rho+3} = [\frac{8}{3\rho + 12}, \frac{3\rho + 4}{3\rho + 12}]. \tag{47}$$

Comparing Eq. (47) with Eq. (35), we find that when $\rho \geq 1$, the motif profile for logistic map is different from the result for *i.i.d.*, which indicates that $\mathbf{Z}^{\rho+3}$ with $\rho > 1$ can capture enough structure for distinguishing both process (see Fig. 5b). Thus, $\mathbf{Z}^{\rho+3}$ contains more structure information than $\mathbf{Z}^3$ [9].

For the $(\rho + 4)-$ node motif, we obtain the following:

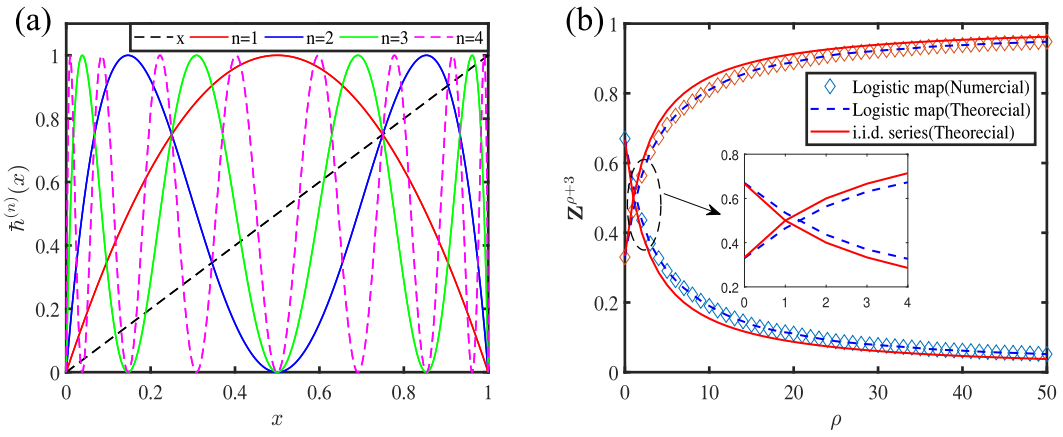

Fig. 5. (a) Plot of the iterates of the chaotic logistic map, (b) $(\rho+3)$-node motif profiles $\mathbf{Z}^{\rho+3}$ associated with logistic map and i.i.d. series.

Theorem 2. *Consider a bi-infinite series of i.i.d. random variable extracted from a continuous distribution $f(x)$ with support (a, b), where $a, b \in \mathbb{R}$. Then the probability of finding $(\rho+4)-$ node motif of LPHVG(ρ) converges to* $\left[\frac{4}{(\rho+3)(\rho+4)}, \frac{1}{\rho+4}, \frac{1}{\rho+4}, 0, \frac{2\rho}{(\rho+3)(\rho+4)}, \frac{\rho+1}{(\rho+3)(\rho+4)}, \frac{\rho+1}{(\rho+3)(\rho+4)}, \frac{\rho(\rho+1)}{(\rho+3)(\rho+4)}\right]$, *i.e.,*

$$\lim_{N\to\infty} \mathbf{Z}^{\rho+4} = \left[\frac{4}{(\rho+3)(\rho+4)}, \frac{1}{\rho+4}, \frac{1}{\rho+4}, 0, \frac{2\rho}{(\rho+3)(\rho+4)}, \frac{\rho+1}{(\rho+3)(\rho+4)}, \frac{\rho+1}{(\rho+3)(\rho+4)}, \frac{\rho(\rho+1)}{(\rho+3)(\rho+4)}\right].$$

Proof. We give the proof for P_I^{1+4} and the proofs for the rest of the probabilities follow analogously. The motif of Type-I of $(\rho+4)-$ node motif of LPHVG(1) (see Fig. 4) can be characterized using a hierarchy of inequalities in the associated time series using the union sets of the nine exclusive inequality sets

$$\begin{aligned} S_I^{1+4} = {} & \{\forall(x_0, x_4), x_1 > x_0, x_2 > x_1, x_3 > x_1\} \cup \{\forall x_0, x_1 > x_0, x_2 > x_1, x_3 < x_1, x_4 < x_3\} \\ & \cup\{\forall x_0, x_1 > x_0, x_0 < x_2 < x_1, x_3 > x_1, x_4 < x_2\} \cup \{\forall x_0, x_1 > x_0, x_0 < x_2 < x_1, x_2 < x_3 < x_1, x_4 < x_2\} \\ & \cup\{\forall x_0, x_1 > x_0, x_0 < x_2 < x_1, x_3 < x_2, x_4 < x_3\} \cup \{\forall x_0, x_1 > x_0, x_2 < x_0, x_3 < x_2, x_4 < x_3\} \\ & \cup\{\forall x_0, x_1 < x_0, x_2 > x_0, x_3 < x_1, x_4 < x_3\} \cup \{\forall x_0, x_1 < x_0, x_1 < x_2 < x_0, x_3 < x_1, x_4 < x_3\} \\ & \cup\{\forall x_0, x_1 < x_0, x_2 < x_1, x_3 < x_2, x_4 < x_3\}. \end{aligned} \tag{48}$$

Thus, using Eq. (27) the probability P_I^{1+4} is expressed

$$\begin{aligned} P_I^{1+4} = {} & \int_a^b f(x_0)dx_0 \int_{x_0}^b f(x_1)dx_1 \int_{x_1}^b f(x_2)dx_2 \int_{x_1}^b f(x_3)dx_3 \int_a^b f(x_4)dx_4 + \int_a^b f(x_0)dx_0 \int_{x_0}^b f(x_1)dx_1 \int_{x_1}^b f(x_2)dx_2 \\ & \times \int_a^{x_1} f(x_3)dx_3 \int_a^{x_3} f(x_4)dx_4 + \int_a^b f(x_0)dx_0 \int_{x_0}^b f(x_1)dx_1 \int_{x_0}^{x_1} f(x_2)dx_2 \int_{x_1}^b f(x_3)dx_3 \int_a^{x_2} f(x_4)dx_4 \\ & + \int_a^b f(x_0)dx_0 \int_{x_0}^b f(x_1)dx_1 \int_{x_0}^{x_1} f(x_2)dx_2 \int_{x_2}^{x_1} f(x_3)dx_3 \int_a^{x_2} f(x_4)dx_4 + \int_a^b f(x_0)dx_0 \int_{x_0}^b f(x_1)dx_1 \int_{x_0}^{x_1} f(x_2)dx_2 \\ & \times \int_a^{x_2} f(x_3)dx_3 \int_a^{x_3} f(x_4)dx_4 + \int_a^b f(x_0)dx_0 \int_{x_0}^b f(x_1)dx_1 \int_a^{x_0} f(x_2)dx_2 \int_a^{x_2} f(x_3)dx_3 \int_a^{x_3} f(x_4)dx_4 \\ & + \int_a^b f(x_0)dx_0 \int_a^{x_0} f(x_1)dx_1 \int_{x_0}^b f(x_2)dx_2 \int_a^{x_1} f(x_3)dx_3 \int_a^{x_3} f(x_4)dx_4 + \int_a^b f(x_0)dx_0 \int_a^{x_0} f(x_1)dx_1 \int_{x_1}^{x_0} f(x_2)dx_2 \\ & \times \int_a^{x_1} f(x_3)dx_3 \int_a^{x_3} f(x_4)dx_4 + \int_a^b f(x_0)dx_0 \int_a^{x_0} f(x_1)dx_1 \int_a^{x_1} f(x_2)dx_2 \int_a^{x_2} f(x_3)dx_3 \int_a^{x_3} f(x_4)dx_4. \end{aligned} \tag{49}$$

Using Eq. (29) with little calculation we obtain

$$P_I^{1+4} = \frac{1}{12} + \frac{1}{40} + \frac{1}{60} + \frac{1}{60} + \frac{1}{40} + \frac{1}{120} + \frac{1}{120} + \frac{1}{120} + \frac{1}{120} = \frac{1}{5}. \tag{50}$$

The equivalence between each motif and its associated inequality set we can also rigorously prove analogously for the other motifs. Table 1 lists all the remaining inequality sets and their corresponding probabilities of LPHVG(1). Thus, we obtain

$$\lim_{N\to\infty} \mathbf{Z}^{1+4} = \left[\frac{1}{5}, \frac{1}{5}, \frac{1}{5}, 0, \frac{1}{10}, \frac{1}{10}, \frac{1}{10}, \frac{1}{10}\right]. \tag{51}$$

Table 1
The rest sets of inequalities and the corresponding probability.

Motif type	Inequality set	Probability
Type-II	$\{\forall x_0, x_1 > x_0, x_2 < x_0, x_3 > x_2, x_4 < x_2\} \cup \{\forall (x_0, x_4), x_1 < x_0, x_2 > x_0, x_3 > x_0\}$ $\cup\{\forall x_0, x_1 < x_0, x_2 > x_0, x_1 < x_3 < x_0, x_4 < x_3\} \cup \{\forall x_0, x_1 < x_0, x_1 < x_2 < x_0, x_3 > x_2, x_4 < x_2\}$ $\cup\{\forall x_0, x_1 < x_0, x_1 < x_2 < x_0, x_1 < x_3 < x_2, x_4 < x_3\} \cup \{\forall x_0, x_1 < x_0, x_2 < x_1, x_3 > x_1, x_4 < x_1\}$ $\cup\{\forall x_0, x_1 < x_0, x_2 < x_1, x_2 < x_3 < x_1, x_4 < x_3\}$	$P_{II}^{1+4} = \frac{1}{5}$
Type-III	$\{\forall x_0, x_1 > x_0, x_2 < x_0, x_3 < x_2, x_3 < x_4 < x_2\} \cup \{\forall x_0, x_1 > x_0, x_0 < x_2 < x_1, x_3 > x_2, x_4 > x_2\}$ $\cup\{\forall x_0, x_1 > x_0, x_0 < x_2 < x_1, x_3 < x_2, x_4 > x_3\} \cup \{\forall x_0, x_1 > x_0, x_2 > x_1, x_3 < x_1, x_4 > x_3\}$ $\cup\{\forall x_0, x_1 < x_0, x_2 > x_1, x_3 < x_1, x_3 < x_4 < x_1\} \cup \{\forall x_0, x_1 < x_0, x_2 < x_1, x_3 < x_2, x_3 < x_4 < x_2\}$	$P_{III}^{1+4} = \frac{1}{5}$
Type-IV	$\{\forall x_0, x_1 < x_0, x_2 = x_1, x_3 = x_1, x_4 > x_1\}$	$P_{IV}^{1+4} = 0$
Type-V	$\{\forall x_0, x_1 > x_0, x_2 < x_0, x_3 > x_0, x_4 > x_2\} \cup \{\forall x_0, x_1 > x_0, x_2 < x_0, x_2 < x_3 < x_0, x_2 < x_4 < x_3\}$ $\cup\{\forall x_0, x_1 < x_0, x_2 < x_1, x_3 > x_1, x_2 < x_4 < x_1\} \cup \{\forall x_0, x_1 < x_0, x_2 < x_1, x_2 < x_3 < x_1, x_2 < x_4 < x_3\}$	$P_{V}^{1+4} = \frac{1}{10}$
Type-VI	$\{\forall x_0, x_1 < x_0, x_2 > x_0, x_1 < x_3 < x_0, x_4 > x_3\} \cup \{\forall x_0, x_1 < x_0, x_1 < x_2 < x_0, x_1 < x_3 < x_2, x_4 > x_3\}$ $\cup\{\forall x_0, x_1 < x_0, x_1 < x_2 < x_0, x_2 < x_3, x_4 > x_2\}$	$P_{VI}^{1+4} = \frac{1}{10}$
Type-VII	$\{\forall x_0, x_1 > x_0, x_2 < x_0, x_3 < x_2, x_4 > x_2\} \cup \{\forall x_0, x_1 < x_0, x_2 > x_1, x_3 < x_1, x_4 > x_1\}$ $\cup\{\forall x_0, x_1 < x_0, x_2 < x_1, x_3 < x_2, x_4 > x_2\}$	$P_{VII}^{1+4} = \frac{1}{10}$
Type-VIII	$\{\forall x_0, x_1 > x_0, x_2 < x_0, x_2 < x_3 < x_0, x_4 > x_3\} \cup \{\forall x_0, x_1 < x_0, x_2 < x_1, x_2 < x_3 < x_1, x_4 > x_3\}$ $\cup\{\forall x_0, x_1 < x_0, x_2 < x_1, x_3 > x_1, x_4 > x_1\}$	$P_{VIII}^{1+4} = \frac{1}{10}$

When $\rho > 1$, we repeat the above proof and finally obtain

$$\lim_{N\to\infty} \mathbf{Z}^{\rho+4} = \left[\frac{4}{(\rho+3)(\rho+4)}, \frac{1}{\rho+4}, \frac{1}{\rho+4}, 0, \frac{2\rho}{(\rho+3)(\rho+4)}, \frac{\rho+1}{(\rho+3)(\rho+4)}, \frac{\rho+1}{(\rho+3)(\rho+4)}, \frac{\rho(\rho+1)}{(\rho+3)(\rho+4)}\right]. \tag{52}$$

Theorems 1 and 2 demonstrate that the $(\rho + 3)$-node and $(\rho + 4)$-node motif profile of LPHVG(ρ) have the unified form for every *i.i.d.* probability distribution $f(x)$. To further check the accuracy of our analytical results, we perform several numerical simulations. We generate a random series of 10^5 data points from uniform, Gaussian white noise, and power-law distributions. Fig. 6(a) shows $(\rho + 3)$-node motif profiles $\mathbf{Z}^{\rho+3}$ associated with uniform distribution (cycles), Gaussian white noise (diamonds) and a power-law distribution (triangles)extracted from LPHVG(ρ) with $\rho = 0, 1, 2, \ldots, 50$. The solid line indicates the theoretical results of Theorem 1. Fig. 6(b) shows the $(\rho + 4)$-node motif profiles $\mathbf{Z}^{\rho+4}$ associated with Gaussian white noise (cycles for Type-I, diamonds for Type-II, squares for Type-III, pentagrams for Type-IV, upper triangles for Type-V, left triangles for Type-VI, stars for Type-VII and crosses for Type-VIII) extracted from LPHVG(ρ) with $\rho = 0, 1, 2, \ldots, 50$. The solid line indicates the theoretical results of Theorem 2. We conclude that the theoretical results agree with the numerics.

Note that a prerequisite for our theoretical results is that the length of the time series must be infinitely long, i.e., have a series size $N \to \infty$, so we assume that the deviation from the theoretical result is due to the effect of finite size. To check the finite size effect, we compute for a series of size N the numeral estimate $\mathbf{Z}^{\rho+3}(N)$ and $\mathbf{Z}^{\rho+4}(N)$ and compare them with the theoretical values. We define the index $\Phi(N)$

$$\Phi(N) = \mathbf{Z}^{\rho+n}(N)/\mathbf{Z}^{\rho+n}. \tag{53}$$

We use $\Phi(N)$ to measure the deviation between the numerical result under a finite size and the theoretical result. Fig. 6(c) plots $\Phi(N) = \mathbf{Z}^{1+3}(N)/\mathbf{Z}^{1+3}$ as a function of the series size N, Fig. 6(d) plots $\Phi(N) = \mathbf{Z}^{1+4}(N)/\mathbf{Z}^{1+4}$ as a function of the series size N. Each dot is averaged over an ensemble of 100 realizations of each size N. The results indicate that a convergence to the asymptotic theory is reached when $N < 10,000$ (we set the value $N = 8728$ in Section 5).

5. A simple application

We use the analytical results of LPHVG(ρ) to distinguish between random and chaotic signals, and we describe the global evolution of crude oil futures [47]. We also describe using DLPHVG(ρ) and ILPHVG$_n$(ρ) to measure real-value time series irreversibility and discriminating between and chaos [48]. Here we describe the application of sequential $(\rho + n)$-node motifs of LPHVG(ρ)and show that $\mathbf{Z}^{\rho+3}$ and $\mathbf{Z}^{\rho+4}$ produce enough information that we can distinguish different processes and thus classify series.

The following are the equations of the continuous dynamical systems we use to generate our flow data. The time series are derived from the x component in each system used to build the corresponding complex network.

To generate a periodic Rossler system we use

$$\dot{x} = -(y + z), \dot{y} = x + ay, \dot{z} = b + (x - c)z. \tag{54}$$

where $a = 0.1, b = 0.1, c = 6$. The sampling interval $T = 0.1$.

To generate a chaotic Lorenz system we use

$$\dot{x} = \sigma(y - x), \dot{y} = x(r - z) - y, \dot{z} = xy - bz. \tag{55}$$

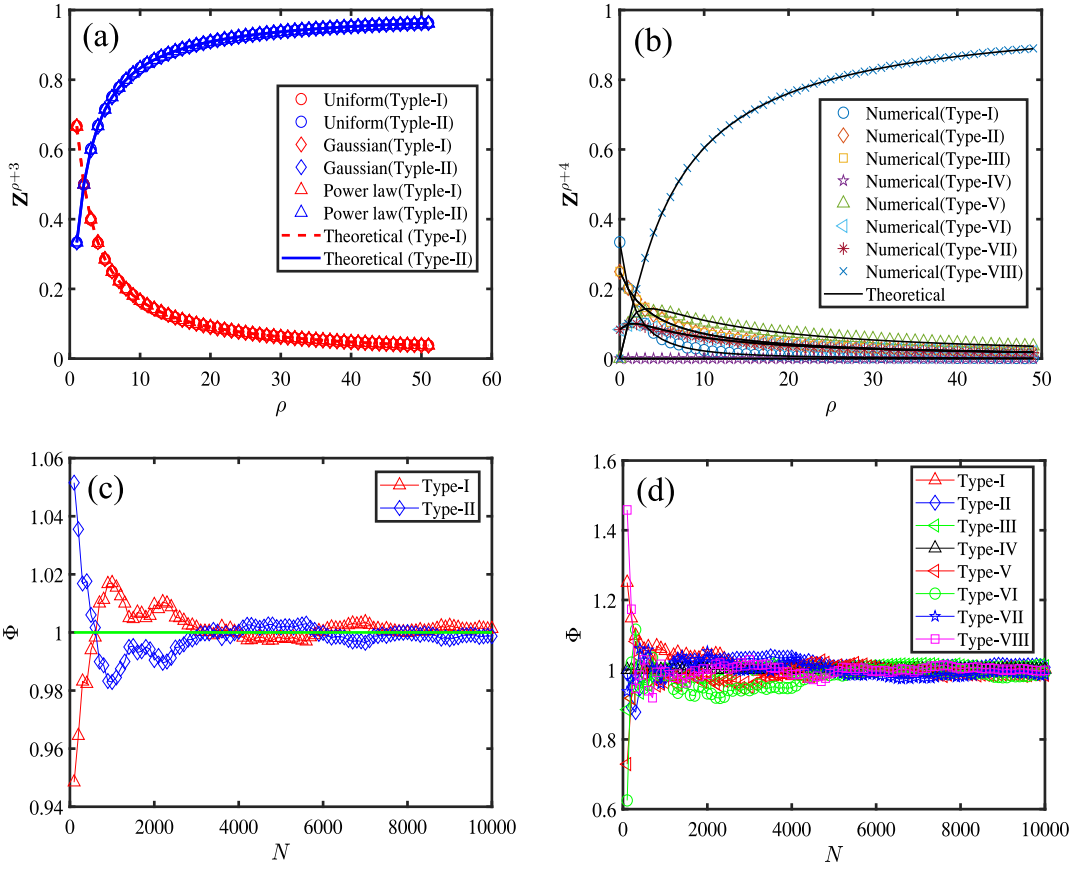

Fig. 6. Numerical simulation results (a) $(\rho+3)$-node motif profiles $\mathbf{Z}^{\rho+3}$ associated with uniform distribution (the cycles), Gaussian white noise (the diamonds) and with a power law distribution (the triangles)extracted respectively from LPHVG(ρ) with $\rho = 0, 1, 2, \ldots, 50$, (b) $(\rho+4)$-node motif profiles $\mathbf{Z}^{\rho+4}$ associated with Gaussian white noise extracted from LPHVG(ρ) with $\rho = 0, 1, 2, \ldots, 50$, (c) The measured frequency of appearance rescaled by its theoretical value $\Phi(N) = \mathbf{Z}^{1+3}(N)/\mathbf{Z}^{1+3}$ is plotted for each motif associated with Gaussian white noise as a function of the time series size N, (d) $\Phi(N) = \mathbf{Z}^{1+4}(N)/\mathbf{Z}^{1+4}$ is plotted for each motif associated with Gaussian white noise as a function of the time series size N. Results are averaged over 100 realizations.

where $\sigma = 10, r = 28, b = 8/3$. The sampling interval $T = 0.05$. We also use data from the U.S. Energy Information Administration (*https://www.eia.gov/dnav/pet/hist/LeafHandler.ashx?n=PET&s=RCLC1&f=D*) on the crude oil future contract 1 (Dollars per Barrel) from 4 April 1983 to 23 Jan 2018 (8728 data points).

To allow comparisons, all the time series associated with different dynamic systems are set at 8728. Fig. 7(a–d) shows the $(\rho+3)$-node motif profiles $\mathbf{Z}^{\rho+3}$ associated with different dynamic systems extracted from LPHVG(ρ) with $\rho = 0, 1, 2, \ldots, 50$. Fig. 7(e) shows the frequency of type-I of $(\rho+3)$-node motif associated with different dynamic systems. Fig. 7(f) shows the frequency of type-I of $(\rho+4)$-node motif associated with different dynamic systems extracted respectively from LPHVG(ρ) with $\rho = 0, 1, 2, \ldots, 50$. The circles indicate a series extracted from a *i.i.d.* Gaussian distribution, and the stars, triangles, and diamonds indicate series extracted from a periodic Rossler system, a chaotic Lorenz system, and a crude oil price series, respectively.

From Fig. 7(a–d) show that the time series associated with different dynamic systems have different $(\rho+3)$-node motif profiles. Fig. 7(e) and (f) show that the frequency of type-I motif of $(\rho+3)$-node motif and $(\rho+4)$-node motif can capture sufficient information to distinguish different processes, i.e., the periodic time series that has the highest frequency of type-I motif, the *i.i.d.* time series that has the lowest frequency, and the frequency of type-I motif associated with chaotic time series is between the periodic time series and the *i.i.d.* time series. Note that these results are only valid when $\rho < 50$, because we selected 8728 to be the length of the time series. Increasing the size of time series increases the corresponding value of ρ.

6. Discussions

We have proposed a novel method for deriving degree distributions of LPHVG(ρ), DLPHVG(ρ) and ILPHVG$_n$(ρ) by using an iterative construction process of LPHVG(ρ), DLPHVG(ρ) and ILPHVG$_n$(ρ) and applying it to an uncorrelated random time

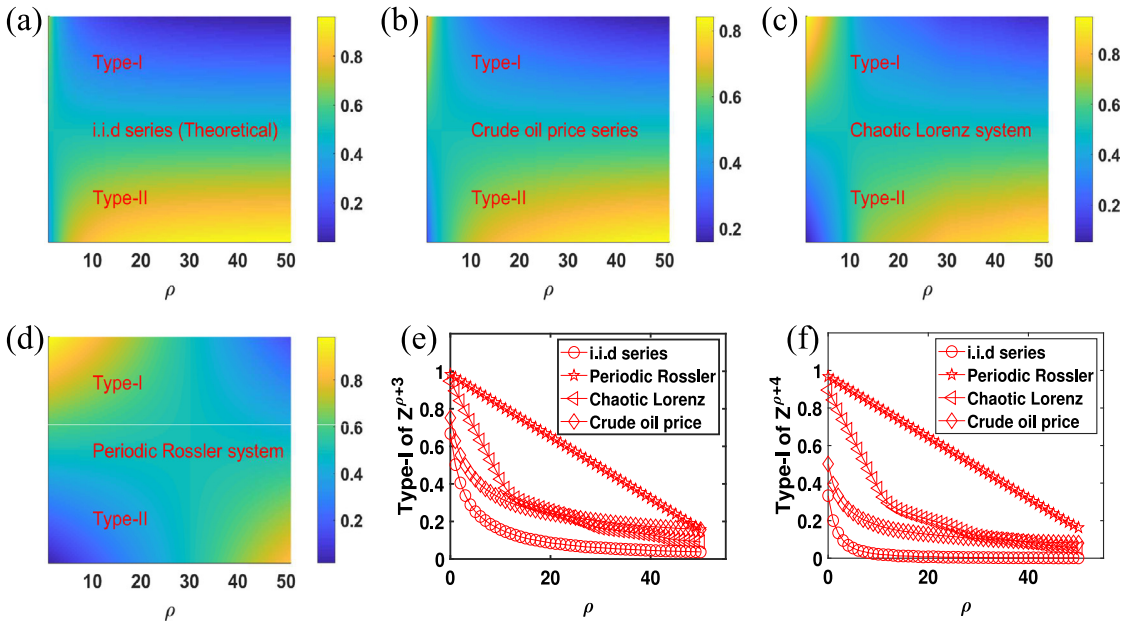

Fig. 7. Numerical simulation results (a)$(\rho+3)$-node motif profiles $\mathbf{Z}^{\rho+3}$ associated with different dynamic systems extracted respectively from LPHVG(ρ) with $\rho = 0, 1, 2, \ldots, 50$, (a) *i.i.d.* time series, (b) crude oil price series, (c)chaotic Lorenz system, (d) periodic Rossler system, (e) the frequency of type-I of $(\rho+3)$-node motif associated with different dynamic systems, (c) $(\rho+4)$-node motif profiles $\mathbf{Z}^{\rho+4}$ associated with different dynamic systems extracted respectively from LPHVG(ρ) with $\rho = 0, 1, 2, \ldots, 50$, (f) the frequency of type-I of $(\rho+4)$-node motif associated with different dynamic systems.

series. We analytically obtain the degree distributions of the LPHVG(ρ), DLPHVG(ρ) and ILPHVG$_n(\rho)$ for random series and find that they are exponential, which confirms prior analytical results using other methods [47,48]. We also introduced the concept of LPHVG(ρ) motifs, which are small subgraphs in which nodes are in consecutive order within the Hamiltonian path that appear at characteristic frequencies for different types of dynamics. We compute the motif profiles for LPHVG(ρ), which is an extension of previous work [9,10]. We find that LPHVG(ρ) motifs provide a mathematically sound, computationally efficient, and highly informative simple feature that can be extracted from any time series. It provides a new way of describing complex signals and their dynamics.

Unsolved problems remain. We still need to develop a theoretical framework for analytically computing the motif profiles of the limited penetrable horizontal visibility graphs associated with such complicated time series as logistic maps and Lorenz equations. We still need research on how to use real data when selecting optimal limited penetrable parameter ρ, how to extend this analysis to the realm of multivariate time series, and how to develop practical applications that will reveal the new dynamic characteristics of the actual system.

Acknowledgments

The Research was supported by the following foundations: The National Natural Science Foundation of China (71503132, 71690242, 91546118), Qing Lan Project of Jiangsu Province (2017), China, University Natural Science Foundation of Jiangsu Province, China (14 kJA110001), Jiangsu Center for Collaborative Innovation in Geographical Information Resource Development and Application, China.

References

[1] A.L. Barabási, R. Albert, Emergence of scaling in random networks, Science 286 (5439) (1999) 509–512.
[2] D.J. Watts, S.H. Strogatz, Collective dynamics of small-world networks, Nature 393 (6684) (1998) 440–442.
[3] M.E.J. Newman, D.J. Watts, Renormalization group analysis of the small-world network model, Phys. Lett. A 263 (4) (1999) 341–346.
[4] P. Erdös, A. Rényi, On the existence of a factor of degree one of a connected random graph, Acta Math. Hungar. 17 (3–4) (1996) 359–368.
[5] L. Lacasa, B. Luque, F. Ballesteros, et al., From time series to complex networks: the visibility graph, Proc. Natl. Acad. Sci. 105 (13) (2008) 4972–4975.
[6] L. Lacasa, On the degree distribution of horizontal visibility graphs associated with Markov processes and dynamical systems: diagrammatic and variational approaches, Nonlinearity 27 (9) (2014) 2063.
[7] B. Luque, L. Lacasa, F. Ballesteros, et al., Horizontal visibility graphs: Exact results for random time series, Phys. Rev. E 80 (4) (2009) 046103.
[8] L. Lacasa, R. Toral, Description of stochastic and chaotic series using visibility graphs, Phys. Rev. E 82 (3) (2010) 036120.
[9] J. Iacovacci, L. Lacasa, Sequential visibility-graph motifs, Phys. Rev. E 93 (4) (2016) 042309.
[10] J. Iacovacci, L. Lacasa, Sequential motif profile of natural visibility graphs, Phys. Rev. E 94 (5) (2016) 052309.
[11] W.J. Xie, R.Q. Han, Z.Q. Jiang, et al., Analytic degree distributions of horizontal visibility graphs mapped from unrelated random series and multifractal binomial measures, Europhys. Lett. 119 (4) (2017) 48008.

[12] R.V. Donner, Y. Zou, J.F. Donges, et al., Recurrence networks a novel paradigm for nonlinear time series analysis, New J. Phys. 12 (3) (2010) 033025.
[13] N. Marwan, J.F. Donges, Y. Zou, et al., Complex network approach for recurrence analysis of time series, Phys. Lett. A 373 (46) (2009) 4246–4254.
[14] R.V. Donner, M. Small, J.F. Donges, et al., Recurrence-based time series analysis by means of complex network methods, Int. J. Bifurcation Chaos 21 (04) (2011) 1019–1046.
[15] A.H. Shirazi, G.R. Jafari, J. Davoudi, et al., Mapping stochastic processes onto complex networks, J. Stat. Mech. Theory Exp. 2009 (07) (2009) P07046.
[16] R. Friedrich, J. Peinke, M. Sahimi, et al., Approaching complexity by stochastic methods: From biological systems to turbulence, Phys. Rep. 506 (5) (2011) 87–162.
[17] J. Zhang, M. Small, Complex network from pseudoperiodic time series: topology versus dynamics, Phys. Rev. Lett. 96 (23) (2006) 238701.
[18] Z. Gao, N. Jin, Complex network from time series based on phase space reconstruction, Chaos 19 (3) (2009) 033137.
[19] X. Xu, J. Zhang, M. Small, Superfamily phenomena and motifs of networks induced from time series, Proc. Natl. Acad. Sci. 105 (50) (2008) 19601–19605.
[20] M. Wang, L. Tian, From time series to complex networks: The phase space coarse graining, Physica A 461 (2016) 456–468.
[21] X. Gao, H. An, W. Fang, et al., Characteristics of the transmission of autoregressive sub-patterns in financial time series, Sci. Rep. 4 (2014).
[22] M. Wang, Non-wandering property of differentiation operator, Int. J. Nonlinear Sci. 6 (1) (2008) 21–28.
[23] X. Gao, H. An, W. Fang, et al., Transmission of linear regression patterns between time series: From relationship in time series to complex networks, Phys. Rev. E 90 (1) (2014) 012818.
[24] M. Wang, Y. Chen, L. Tian, et al., Fluctuation behavior analysis of international crude oil and gasoline price based on complex network perspective, Appl. Energy 175 (2016) 109–127.
[25] Z. Zhang, M. Wang, L. Tian, et al., Research on the development efficiency of regional high-end talent in China: A complex network approach, PLoS One 12 (12) (2017) e0188816.
[26] Z. Zhang, M. Wang, H. Xu, et al., Research on the co-movement between high-end talent and economic growth: A complex network approach, Physica A 492 (2018) 1216–1225.
[27] H. Chen, L. Tian, M. Wang, et al., Analysis of the dynamic evolutionary behavior of american heating oil spot and futures price fluctuation networks, Sustainability 9 (4) (2017) 574.
[28] Z.K. Gao, Y.X. Yang, P.C. Fang, et al., Multiscale complex network for analyzing experimental multivariate time series, Europhys. Lett. 109 (3) (2015) 30005.
[29] J. Xiao, M. Wang, L. Tian, et al., The measurement of China's consumer market development based on CPI data, Physica A 490 (2018) 664–680.
[30] Z.K. Gao, S.S. Zhang, W.D. Dang, et al., Multilayer network from multivariate time series for characterizing nonlinear flow behavior, Int. J. Bifurcation Chaos 27 (04) (2017) 1750059.
[31] L. Lacasa, V. Nicosia, V. Latora, Network structure of multivariate time series, Sci. Rep. 5 (2015).
[32] M. Wang, L. Tian, Du R., Research on the interaction patterns among the global crude oil import dependency countries: A complex network approach, Appl. Energy 180 (2016) 779–791.
[33] R. Du, Y. Wang, G. Dong, et al., A complex network perspective on interrelations and evolution features of international oil trade, 2002–2013, Appl. Energy 196 (2017) 142–151.
[34] M. Wang, L. Tian, H. Xu, et al., Systemic risk and spatiotemporal dynamics of the consumer market of China, Physica A 473 (2017) 188–204.
[35] M. Wang, Tian L., Regulating effect of the energy market theoretical and empirical analysis based on a novel energy prices energy supply economic growth dynamic system, Appl. Energy 155 (2015) 526–546.
[36] H. An, X. Gao, W. Fang, et al., Research on patterns in the fluctuation of the co-movement between crude oil futures and spot prices: A complex network approach, Appl. Energy 136 (2014) 1067–1075.
[37] G.J. Wang, C. Xie, H.E. Stanley, Correlation structure and evolution of world stock markets: Evidence from Pearson and partial correlation-based networks, Comput. Econ. 51 (3) (2018) 607–635.
[38] G.J. Wang, C. Xie, S. Chen, Multiscale correlation networks analysis of the US stock market: a wavelet analysis, J. Econ. Interact. Coord. 12 (3) (2017) 561–594.
[39] G.J. Wang, C. Xie, K. He, et al., Extreme risk spillover network: application to financial institutions, Quant. Finance 17 (9) (2017) 1417–1433.
[40] M. Wang, L. Zhao, R. Du, et al., A novel hybrid method of forecasting crude oil prices using complex network science and artificial intelligence algorithms, Appl. Energy 220 (2018) 480–495.
[41] M. Wang, L. Tian, P. Zhou, A novel approach for oil price forecasting based on data fluctuation network, Energy Econ. 71 (2018) 201–212.
[42] T.T. Zhou, N.D. Jin, Z.K. Gao, et al., Limited penetrable visibility graph for establishing complex network from time series, Acta. Phys. Sin. 61 (3) (2012) 1–11.
[43] Z.K. Gao, L.D. Hu, T.T. Zhou, et al., Limited penetrable visibility graph from two-phase flow for investigating flow pattern dynamics, Acta Phys. Sin. 62 (11) (2013) 1–11.
[44] Z.K. Gao, Q. Cai, Y.X. Yang, et al., Multiscale limited penetrable horizontal visibility graph for analyzing nonlinear time series, Sci. Rep. 6 (2016) 35622.
[45] J. Wang, C. Yang, R. Wang, et al., Functional brain networks in Alzheimer's disease: EEG analysis based on limited penetrable visibility graph and phase space method, Physica A 460 (2016) 174–187.
[46] R.X. Wang, J.M. Gao, Z.Y. Gao, et al., Complex network theory-based condition recognition of electromechanical system in process industry, Sci. China Technol. Sci. 59 (4) (2016) 604–617.
[47] M. Wang, A.L.M. Vilela, R. Du, et al., Exact results of the limited penetrable horizontal visibility graph associated to random time series and its application, Sci. Rep. 8 (1) (2018) 5130.
[48] M. Wang, A.L.M. Vilela, R. Du, et al., Topological properties of the limited penetrable horizontal visibility graph family, Phys. Rev. E (2018).